THE PENNSYLVANIA STATE UNIVERSITY
SCHREYER HONORS COLLEGE

DEPARTMENT OF AEROSPACE ENGINEERING

Autopilot Design for the Takeoff and Landing of a Tailwheel Airplane

GRACELYNE H. ALLRED
SPRING 2021

A thesis
submitted in partial fulfillment
of the requirements
for a baccalaureate degree
in Aerospace Engineering
with honors in Aerospace Engineering

Reviewed and approved* by the following:

Mark D. Maughmer
Professor of Aerospace Engineering
Thesis Supervisor and Honors Advisor

Sven Schmitz
Associate Professor of Aerospace Engineering
Faculty Reader

* Electronic approvals are on file.

ABSTRACT

This work seeks to design and verify a flight control solution, using an adaptive control architecture, for the takeoff and landing of an autonomous fixed-wing vehicle with conventional gear. The International Aerial Robotics Competition (IARC) challenges teams to develop autonomous platforms to accomplish missions with problems not previously solved. The Pennsylvania UAV Research Lab (PURL) is competing in IARC's Mission 9, which partially requires high-speed flight with a large payload. The SIG Rascal 168, a radio-controlled aircraft with conventional gear, is the chosen platform and has motivated the model development and controller design presented in this work. The typical control challenges of this tailwheel aircraft, intensified by the added payload, make this vehicle a useful flight-test platform. This thesis presents the integration of the aircraft model into a previously developed flight simulation environment that uses a neural network-based adaptive flight controller to refine flight characteristics during specific mission phases, including take-off and landing. The resulting autopilot design is evaluated in simulation and prepared to be incorporated with the necessary hardware onboard Rascal 168.

TABLE OF CONTENTS

LIST OF FIGURES

LIST OF TABLES

ACKNOWLEDGEMENTS

There are so many people who have made a profound impact on me during these last 4 years at Penn State. I am so grateful for these individuals who continually inspire and challenge me to grow as an engineer and person. I must thank Rachel Axten for her readily given guidance and relentless work on the flight test vehicle throughout this project. Her friendship made the late nights not so late and any unanticipated challenges not so stressful. I would like to thank Venkat Iyer for all his help dissecting the simulation software used for the project. I do not know where else I could have gained this knowledge of the architecture. I would also like to thank Dr. Eric Johnson for helping me generate this idea and providing unique platforms to explore this research area.

I must acknowledge my honors advisor, Dr. Mark Maughmer. He has been an unwavering advocate and persistent source of wisdom since I first arrived at Penn State. I appreciate the many times he has challenged my understanding and encouraged me to think more critically. Several others connected to the Sailplane class community have always made time to answer my every question and connect me with helpful resources. I must give a big thank you to both Chris Axten and Len Metkowski for their insight and patience.

In addition to these individuals, I am very grateful for the many faculty and staff within the aerospace department that work tirelessly to prepare students for success in the aerospace industry. Thank you, Dr. Sven Schmitz, for your readiness to become a reader and provide feedback on such short notice. I would like to thank the several professors within the aerospace department who rapidly mobilized to provide me with resources and guidance in the final weeks of my thesis writing.

Chapter 1: Introduction

1.1 Problem Statement

Before the 1950s, the majority of airplanes were manufactured with the main gear forward of a skid or wheel located at the tail. These airplanes, known as taildraggers or tailwheel aircraft, are still used for a variety of applications despite the more common design preference of tricycle landing gear. On a taildragger, the long moment arm from the main gear to the tail allows a smaller, lighter support mechanism. The aircraft also naturally rests in a nose-high attitude, which keeps the propeller away from debris on rough surfaces. This natural nose-high attitude is also ideal for an aircraft that needs to take off and land in short distances, enabling a slower touchdown speed at a high pitch angle without damaging the tail. Although the tricycle gear configuration is now more prevalent, the challenges of directional control in a tailwheel aircraft still exist, specifically for tailwheel pilots and engineers seeking to develop autonomous platforms. These control challenges, which exist primarily on the ground, involve its directional instability, weathervaning tendency, and its nose-high attitude at rest.

Tailwheel aircraft are inherently unstable on the ground because their center of gravity is located behind the main gear, its pivot point. This means that any deviation from movement parallel to the aircraft longitudinal axis will be exacerbated and its forward momentum will instigate rotation about the vertical and longitudinal axis. When not anticipated and corrected, this movement commonly manifests itself as a "ground loop" during landing roll.

Tailwheel aircraft are also much more sensitive to any surface wind when compared to the more contemporary tricycle gear configuration. A free moving tailwheel allows the aircraft to easily swing the nose into any slight wind that perturbs it from its unstable equilibrium. A nose-high attitude on the ground puts the aircraft at an initially higher angle of attack than most tricycle-gear aircraft, which can even allow it to asymmetrically lift off during a strong gust of wind.

1.2 Research Significance

Autonomous fixed-wing vehicles have the potential to perform a diverse array of missions related to scientific exploration, defense, commercial infrastructure, and healthcare, many of which are not yet possible. When compared to a single or multirotor system, a fixed-wing vehicle is generally capable of covering longer distances, reaching higher flight speeds, and loitering longer because of its aerodynamic efficiency. This makes fixed-wing autonomous vehicles useful for transport, aerial mapping, and atmospheric research. These vehicles must often be adapted from radio controlled or remotely piloted platforms to simplify the manufacturing process and reduce cost when aerodynamic performance is not the primary area of investigation. Small radio-controlled aircraft are often the ideal candidates to test autonomous control methods and performance. Many easily assembled radio-controlled aircraft feature the tailwheel gear configuration. The work in this paper will reveal the challenges of integrating autonomous flight control in such vehicles.

The Pennsylvania UAV Research Lab (PURL) is competing in the International Aerial Robotics Competition (IARC) Mission 9. Part of the team's design solution requires the use of a large radio-controlled airplane that must conduct fast outdoor operations over a long distance and precisely manipulate a large object. The SIG Rascal 168, an easy-build, radio-controlled (RC) tailwheel aircraft, was determined to be the ideal platform for this mission. The work presented in this thesis will assist the team effort to complete IARC Mission 9 and enable future autonomous applications of RC tailwheel aircraft at PURL.

1.3 Research Objectives

- Investigate the longitudinal and lateral-directional control challenges of an autonomous fixed-wing vehicle with conventional gear.

- Develop a flight control solution for the takeoff and landing of this vehicle using an adaptive control architecture and simulation environment with hardware in the loop.
- Expand the autonomous capabilities of tailwheel platforms for research applications.

1.4 Methodology

The dynamic model of the SIG Rascal 168 aircraft was refined using the simulation platform known as the Penn State/Georgia Tech UAV Simulation Tool (PS/GUST). Extensive discussion and experimentation with the tool's interface was required to learn its setup and architecture. A previously developed fixed-wing model within the tool was adapted to approximate the Rascal 168. The aircraft manufacturer provided some initial airframe dimensions, but no quantifiable information on the aircraft aerodynamic characteristics, performance, or stability behavior. Therefore, physical measurements of the aircraft were taken at PURL and used to inform the model. Stability characteristics and coefficients were predicted using an approximate aircraft geometry in Drela and Youngren's aerodynamic analysis program, Athena Vortex Lattice (AVL) [1]. This estimated dynamic model was used as a starting point for the neural network-based flight controller within PS/GUST. Gain values were determined by iterating gain and flight profile changes and evaluating the resulting flight characteristics.

Chapter 2:

Background

2.1 International Aerial Robotics Competition

The AUVSI International Aerial Robotics Competition (IARC) is an event that challenges teams to take on design tasks previously thought impossible. At each event, participants move aerial robotics forward by attempting to solve significant and useful mission challenges. IARC Mission 9 requires a fully autonomous aerial robot with self-contained computing to complete a series of complex tasks. A portion of the mission requires the system to fly 3 km in at least 9 minutes. The aerial robot can be of any configuration, rotary wing, fixed-wing, or other, and can even include a "mothership" with expendable air-launchable subvehicles. The PURL team previously determined that an autonomous fixed-wing mothership, carrying an expendable rotary wing vehicle, was the ideal configuration for their design solution, which provides the context for this research.

2.2 Aircraft Test Platform

The SIG Rascal 168 radio-controlled (RC) aircraft is self-assembled from laser cut plywood and balsa pieces, assembled using cyanoacrylate adhesive. SIG Rascal aircraft have been used by other universities, such as Embry–Riddle Aeronautical University [2] and the Air Force Institute of Technology [3], to develop autonomous control solutions. Figure 1 features the completed Rascal 168.

Figure 1: SIG Rascal 168

2.2.1 Configuration Layout

The Rascal 168 is a high wing monoplane that features a conventional tail arrangement and tailwheel landing gear configuration. Figure 2 and Figure 3 reveal the top and side views of the aircraft.

Figure 2: SIG Rascal 168 Top View

Figure 3: SIG Rascal 168 Side View

The manufacturer provided initial values for wing area and span. Table 1,Table 2, and Table 3 specify the measured wing and tail dimensions recorded at PURL.

Table 1: Wing Dimensions

Wing	*Measurement*
S	3710 in^2
b	14 ft
c_r	2.0 ft
c_t	0.75 ft
Dihedral	2 deg
i	0 deg

Table 2: Horizontal Tail Dimensions

Horizontal Tail	*Measurement*
S_{ht}	474 in^2
b_{ht}	55.5 in
$c_{r_{ht}}$	9.5 in
$c_{t_{ht}}$	7.5 in

Table 3: Vertical Tail Dimensions

Vertical Tail	*Measurement*
S_{vt}	250 in^2
b_{vt}	18 in
$c_{r_{vt}}$	18 in
$c_{t_{vt}}$	9.5 in

2.2.2 Airfoil and Wing Geometry

The Rascal 168 wing features a nearly elliptical planform with a straight leading edge as seen in Figure 2. The mean aerodynamic chord ($\bar{c}$), distance from $\bar{c}$ to the aircraft centerline ($\bar{y}$), and taper ratio (λ) were calculated from the dimensions given prior in Table 1. The aspect ratio (AR) was calculated using

$$AR = \frac{b^2}{S}$$

Table 4 reveals the parameter values used for stability analysis and the aircraft dynamic model.

Table 4: Wing Geometry Parameters

Parameter	*Value*
$\bar{c}$	1.68 ft
$\bar{y}$	5.125 ft
AR	7.61
λ	0.375

The manufacturing company did not provide airfoil information for the Rascal 168 model. Therefore, an airfoil profile was approximated using the SIG Rascal 110 aircraft information collected by Jodeh, Nidal, Paul Blue, and Athon Waldron [3]. The Rascal 168 airfoil profile closely matches the Eppler E193 airfoil. Figure 4 depicts the airfoil profile, which has a max thickness of 10.2% at 31% chord and a max camber of 3% at 44.7% chord.

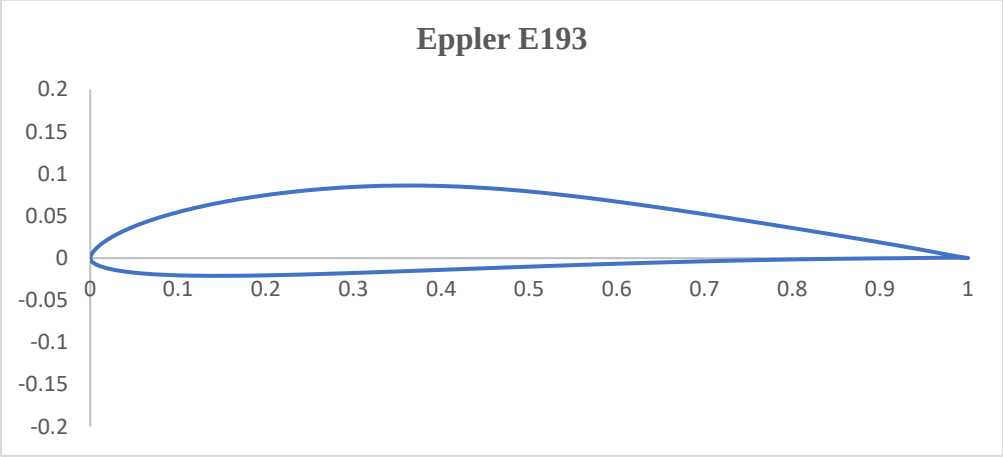

Figure 4: Airfoil Profile

According to XFOIL [4] results, the Eppler E193 airfoil has a $c_{l_{max}}$ close to 1.3 at Reynolds numbers ranging from 500,000 to 1,000,000.

2.2.3 Propulsion System

The test aircraft thrust is provided by an ElectriFly Rimfire 65cc 160Kv Brushless electric motor, two Turnigy 16000mAhr 6S 12C LiPo batteries in series, Castle Creations Talon 120HV ESC, and a fixed-pitch Aerostar Electric Series Wood 24x12 Propeller. The chosen battery cell type discharges at 12C constant and 24C burst, with the 65cc motor system. The maximum continuous power, output by this electric motor, is 7500W. Propeller angular velocity at full power was determined to be roughly 5000 rpm. Propeller twist was calculated from the propeller pitch specification of 12 in of advance per revolution using [5]

$$\theta_1 = -\frac{4}{3}\tan^{-1}\left(\frac{pitch}{2\pi\frac{3}{4}r}\right)$$

Assuming 85% efficiency, the maximum Torque was determined by

$$Q_{max} = 0.85\ \frac{P_{max}}{\Omega}$$

The specified and calculated propulsion parameters useful for the aircraft dynamic model are listed in Table 5.

Table 5: Propulsion Model Parameters

System Specification	*Value*
$\boldsymbol{r}$	12 in
$\boldsymbol{\Omega}$	7000 rpm
$\boldsymbol{\theta_1}$	0.36 radians
$\boldsymbol{Q_{max}}$	6.4 ft-lb

2.2.4 Weight and Inertia Properties

The SIG Rascal 168 empty weight varies based on manufacturing nuances between 40lb and 44lb, according to the manufacturer. The aircraft assembled at PURL was modified from the original assembly instructions to include the slightly heavier propulsion system, as specified in Section 2.2.3. The final weight of the assembled aircraft was found to be 50 lb with the center of gravity located at roughly 25% chord.

No inertia information was available for Rascal 168 from the manufacturer. Rough estimates were made based on similarly dimensioned RC aircraft. Precise calculation of inertial information was not necessary because the chosen controller adapts actively to error in the aircraft model as later described in Section 3.2.3. The estimated inertia information used for the simulation model are specified in Table 6.

Table 6: Moments and Products of Inertia

Plane of Symmetry	***Inertia (slug-ft^2)***
J_X	20.0
J_Y	9.0
J_Z	22.0
J_{XZ}	0.0

2.2.5 Aerodynamic and Performance Predictions

The wing and tail geometry were modeled in Drela and Youngren's Athena Vortex Lattice (AVL) [1] to investigate the Rascal 168 aerodynamic characteristics. The aircraft partial elliptical planform was approximated as a double tapered wing, incorporating the E193 airfoil. The rounded horizontal and vertical stabilizers were approximated as single tapered surfaces. This geometry is presented in Figure 5.

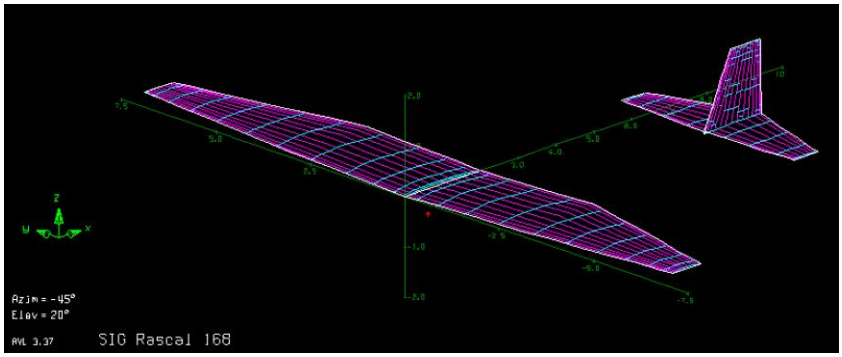

Figure 5: Aircraft AVL Geometry

To predict stall onset, AVL cases were executed using varying airspeeds to generate a c_l distribution across the span and used to calculate aircraft c_L and α. The Treffz plot of the aircraft lift distribution at an airspeed of 37 ft/s with untrimmed moments is depicted in Figure 6. At this flight condition the aircraft angle of attack is calculated to be between 11 and 12 degrees.

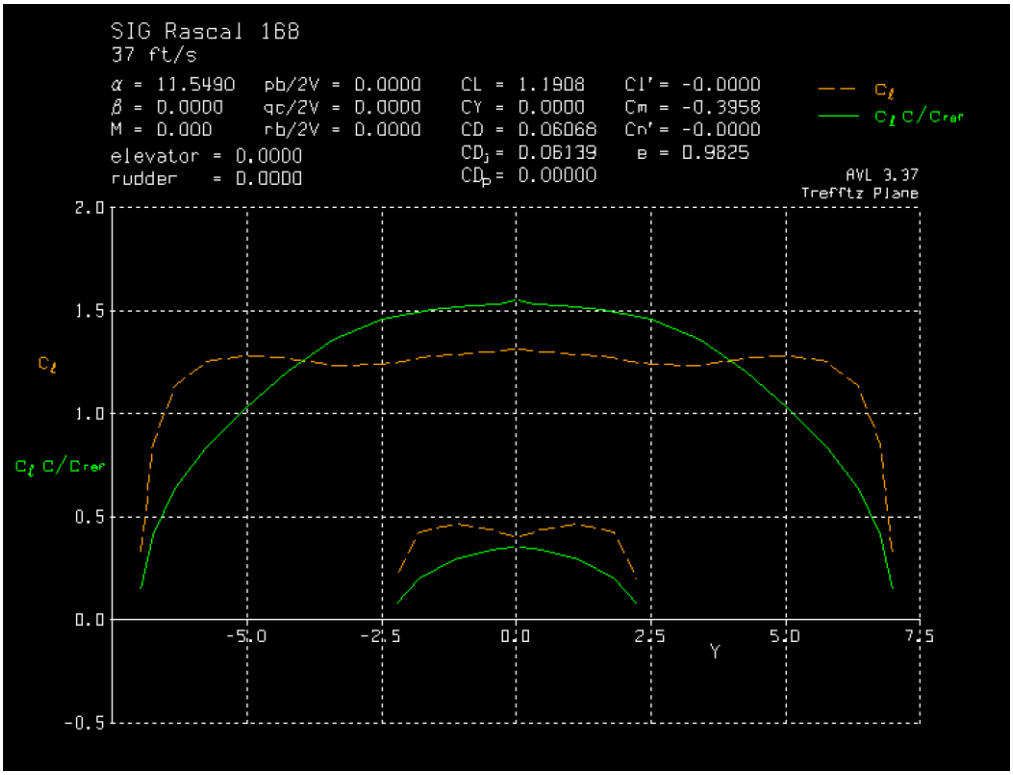

Figure 6: Spanwise Lift Distribution at a Flight Condition Approaching Stall

As indicated by the yellow dashed line, at an aircraft c_L of 1.19, much of the wing is close to or has already exceeded the E193 two-dimensional $c_{l_{max}}$ and stall is imminent.

Another case was executed to justify a flight speed of 60 ft/s for the purpose of stability calculations. At this speed, the aircraft α was around 1.5 degrees at a c_L of 0.37. The lift curve slope was 4.8 rad^{-1}. These parameters were well within the bounds anticipated by the PURL team and necessary for the completion of IARC Mission 9.

2.2.6 Stability Analysis

Further investigation into the Rascal 168 stability characteristics was made using AVL. The parameters described previously were used to specify the necessary flight conditions for analysis. The neutral point was calculated to be 1.25 ft behind the leading edge. The static stability coefficients necessary for the aircraft model are listed in Table 7.

Table 7: Static Stability Coefficients

COEFFICIENT	VALUE
C_{M_0}	0.0168
C_{M_α}	-1.868
C_{M_Q}	-31.06
C_{Y_β}	-0.1262
C_{Y_P}	0.0237
C_{Y_R}	0.1541
C_{l_β}	-0.00118
C_{l_P}	-0.4364
C_{l_R}	0.0819
C_{N_β}	0.0709
C_{N_P}	-0.0223
C_{N_R}	-0.0896
$C_{M_{\delta_e}}$	-0.813
$C_{l_{\delta_r}}$	0.00115
$C_{N_{\delta_r}}$	-0.0329

Chapter 3:

Model Development

3.1 Dynamic Model

3.1.1 Assumptions

The fixed-wing model was assumed to be perfectly symmetric across all three axes, by setting the three products of inertia equal to zero, as commonly done for dynamic models of small radio-controlled aircraft. The equations were further simplified by assuming a flat earth.

3.1.2 Equations of Motion

The nonlinear representation of a fixed-wing aircraft, later used to model Rascal 168 flight characteristics, is previewed below. These equations use the body-fixed, wind-axis, and inertial coordinate system described by Stevens, Brian L., Frank L. Lewis, and Eric N. Johnson [5].
Aircraft forces are calculated as given by

$$\dot{U} = RV - QW - g_D sin\theta + \frac{X_A + X_T}{m}$$

$$\dot{V} = -RU - PW + g\_D\ sin\phi\ cos\theta + \frac{(Y_A + Y_T)}{m}$$

$$\dot{W} = QU - PV + g_D cos\phi\ cos\theta + \frac{Z_A + Z_T}{m}$$

Moment equations implemented are described using

$$\Gamma\dot{P} = J_{xz}\left[J_x - J_y + J_z\right]PQ - \left[J_z\left(J_z - J_y\right) + J_{xz}^2\right]QR + J_z l + J_{xz} n$$

$$J_y\dot{Q} = (J_z - J_x)PR - J_{xz}(P^2 - R^2) + m$$

$$\Gamma\dot{R} = \left[(J_x - J_y)J_x + J_{xz}^2\right]PQ - J_{xz}\left[J_x - J_y + J_z\right]QR + J_{xz} l + J_x n$$

$$\Gamma = J_x J_z - J_{xz}^2$$

3.2 Simulation Environment

The aircraft autopilot development was accomplished using a Hardware in the Loop (HITL) simulation environment, the Penn State/Georgia Tech UAV Simulation Tool (PS/GUST) [6]. This tool emulates sensor and actuator behavior, which acts as the interface between the aircraft dynamic model and controller being tested. PS/GUST's three major components include a ground control station, dynamic and sensor models, and onboard flight code. PS/GUST's HITL structure, used to evaluate changes to the flight code, is portrayed in Figure 7 [7].

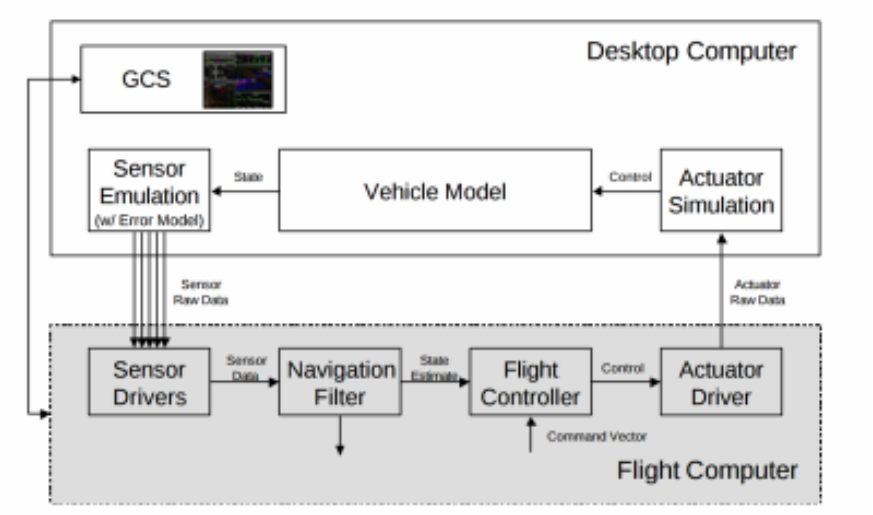

Figure 7: Hardware in the Loop Testing Structure

In addition to vehicle dynamics, the vehicle model includes the mathematical representation of external actions such as actuator movement and GPS error. This allows the plant simulation to electrically imitate sensor data and error encountered in the real world. These signals are read by the embedded controller that prompt it to implement its control algorithms. Because PS/GUST provides a ground control station and systems management, the tool can also be simply used for general vehicle simulation and flight operations.

3.2.3 Adaptive Control Architecture

PS/GUST implements a flight control architecture that uses a neural network based adaptive controller developed by Johnson and Kannan [8]. The controller uses dynamic inversion, or feedback linearization [5], and Pseudo Control Hedging [9], which prevents the plant from learning unwanted behavior.

Typical linear control involves finding desirable operating points within the flight envelope and linearizing the model at those points. Separate linear flight controllers are then designed for operation around each of these points. This process, known as Gain Scheduling, organizes gains for each flight condition and retrieves them when the vehicle nears that operating point. This can become cumbersome when the vehicle has a large operating envelope, many failure modes, or high uncertainty in its dynamic model. The number of designed and scheduled gains becomes so large it degrades system performance. These issues are avoided using adaptive control, which refines the controller response to unmodelled dynamics in real time, including non-linearities, changes in vehicle behavior due to failures, and unexpected changes in the flight environment. With adaptive control, one controller can be used for all flight conditions. An artificial neural network can be trained to adapt a controller for nonlinear behavior using dynamic inversion. Dynamic inversion allows the expected and actual vehicle response to be compared by establishing a reference model that identifies the vehicle's desired aircraft state. An inverted model of the vehicle's dynamics then identifies control inputs required to control the vehicle towards that desired state. This is called 'dynamic inversion' because the neural network dynamically monitors whether the vehicle responds to control inputs as expected and linearizes the measured deviation from that model before it is sent to the adaptive element, which determines the optimal gain adjustments.

Adaptive control can become problematic if no limitations are put on model refinement near the edges of the aircraft flight envelope. For instance, an aircraft with a control surface already fully deflected could be commanded by the controller to place the aircraft in a condition outside its capability. Johnson

and Kannan's implementation [8] uses Pseudo Control Hedging (PCH) to prevent adaption to plant input characteristics by allowing the reference model to only call for desired aircraft states that are within the flight envelope.

3.2.4 Tailwheel Aircraft Implementation

The nonlinear representation of a fixed-wing aircraft, explained earlier in the chapter, had been previously modeled in PS/GUST for application on more generic fixed-wing platforms. The model was adjusted to match the SIG Rascal 168 characteristics described in Section 2.2. Linear controller gains were initially refined to determine a baseline for the adaptive controller within PS/GUST.

First, gains that related thrust to forward, lateral, and vertical acceleration were roughly adjusted to offset oscillation at a commanded cruise condition. Then, gains that directly affected control surface response were scaled in shallow turns and steady level flight, reducing oscillatory response until it was not readily apparent to an outside observer. This allowed attention to be moved to the primary challenges of tailwheel aircraft control.

All the undesirable consequences of lateral-directional instability on the ground result from any combination of the following actions:

- not enough control authority being applied
- slow response to rapidly changing movement.
- uncorrected steady state error due to the airplanes natural flying characteristics

For the tailwheel pilot, this translates to more aggressive rudder deflection on the ground at low airspeeds (proportional gain), higher pressure on both rudder petals (derivative gain), quicker response time (derivative gain), and being intentional about flying precisely (integral gain) during takeoff and landing. Very small steady state sideslip angles are typical of fixed-wing flight. These are due to forces from the propulsion system, slipstream aerodynamic effects, and asymmetric aspects of the aircraft shape. These

aspects are incorporated into PS/GUST's generic fixed wing model. The original fixed-wing controller in PS/GUST paid very little attention to reducing sideslip angle (β) during most phases of flight. This made sense for the generic model because a small β angles are not an issue for airplanes with tricycle landing gear until they become large enough to decrease aerodynamic performance or damage the landing gear. Therefore, gains relating rudder and aileron movement to β and lateral acceleration were adjusted, adding integral gain to reduce steady state error. Derivative gains responding to β were increased to damp out induced oscillation and keep $\dot{\beta}$ near zero. Another rudder integrator, that turns on just above flare velocity, was activated to further react to lateral acceleration just before touchdown and during roll out. Because control effectiveness decreases at slow speeds, this integrator uses a much higher proportional gain for lateral acceleration. The final gain values, used to obtain the simulated controller performance presented in Section 4.1, are detailed in Table 8.

Table 8: Baseline Proportional, Derivative, and Integral Gains

Gain	*Value*
$\boldsymbol{k_{d_\phi}}$	0.9
$\boldsymbol{k_{p_\phi}}$	1.1
$\boldsymbol{k_{i_\phi}}$	1
$\boldsymbol{k_{d_\alpha}}$	1
$\boldsymbol{k_{p_\alpha}}$	1.3
$\boldsymbol{k_{i_\alpha}}$	0.8
$\boldsymbol{k_q}$	0
$\boldsymbol{k_{d_\beta}}$	1.3
$\boldsymbol{k_{p_\beta}}$	1.5
$\boldsymbol{k_{i_\beta}}$	1.2
$\boldsymbol{k_{p_{a_x}}}$	0.003
$\boldsymbol{k_{i_{a_x}}}$	1
$\boldsymbol{k_{p_{a_y}}}$	20
$\boldsymbol{k_{p_{a_{yg}}}}$	100
$\boldsymbol{k_{i_{a_y}}}$	1
$\boldsymbol{k_{p_{a_z}}}$	35
$\boldsymbol{k_{i_{a_z}}}$	1
$\boldsymbol{k_{ar}}$	0.25

Finally, the aircraft approach profile was made more like that of a full-scale tailwheel aircraft. Approach profiles for other fixed-wing models in PS/GUST specify touchdown speeds much higher than stall speed with very little nose up attitude in the flare. A fast touchdown speed allows for more control authority, an easily stabilized approach, and a smoother reduction of vertical speed. Since all aerodynamic moments are proportional to airspeed, it is important that an aircraft, unstable in yaw and roll after touchdown, land as slow as possible. It is also most ideal for tailwheel aircraft to land in a nose high attitude where all three wheels can make ground contact simultaneously. When the tailwheel is in contact with the ground, it helps resist rotation about the vertical axis when the airplane is perturbed from equilibrium. The approach profile of the Rascal 168 will later be compared to that of a generic fixed-wing aircraft, having tricycle landing gear, which was already implemented in the simulation tool. The primary trajectory parameters that were adjusted to obtain the appropriate approach profile for the simulated model of Rascal 168 are listed in Table 9. Because PS/GUST is set up to have the vehicle slowly decelerate on approach, unlike a typical piloted approach, transition to flare is made when a certain airspeed is reached. Flare rotation velocity is the airspeed the vehicle is commanded to transition to the desired angle of attack at touchdown. The rate at which this rotation is accomplished is determined by the flare vertical acceleration. Flare vertical acceleration is positive upward to arrest the aircraft descent and achieve the desired vertical speed at touchdown. Flare velocity deceleration notes the rate at which airspeed is reduced in the flare.

Table 9: Rascal 168 Desired Flare Characteristics

Parameter	*Value*
Flare Rotation Velocity	37 ft/s
Flare Vertical Acceleration	5 ft/s^2
Flare Velocity Deceleration	2 ft/s^2
Desired Vertical Speed at Touchdown	0 ft/s
Desired $\boldsymbol{\alpha}$ at Touchdown	0.11 radians

Chapter 4: Performance Results

4.1 Simulated Autopilot Performance

The simulated aircraft behavior when commanded to takeoff, fly a rectangular path, and return to land is shown in Figure 8. The purple path and circular waypoints denote the commanded trajectory of the airplane. The yellow line represents the simulated response of the aircraft to controller inputs.

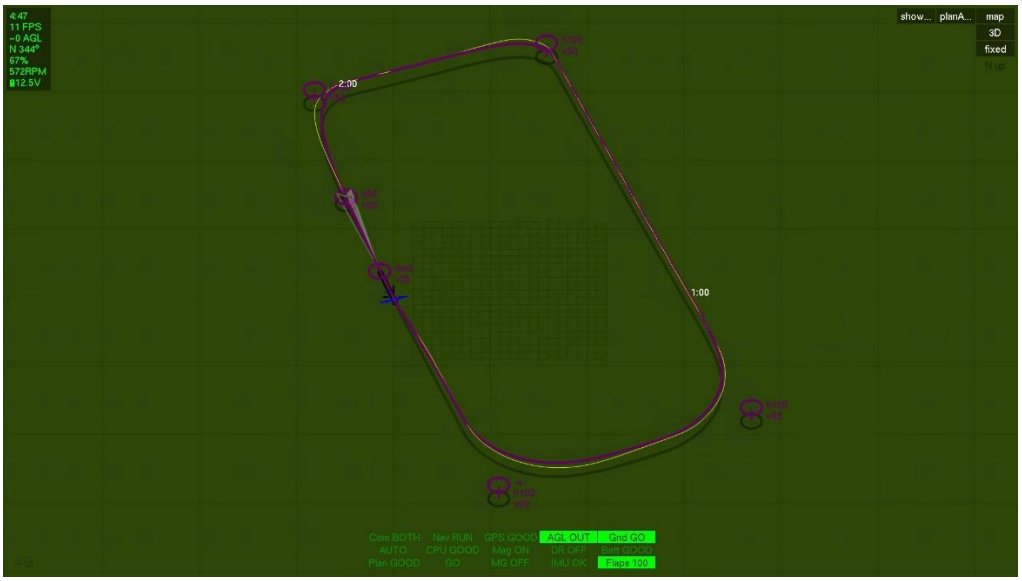

Figure 8: Commanded vs Actual Flight Path in the Traffic Pattern

4.1.1 Takeoff and Departure

Simulated takeoff and departure was examined by commanding the aircraft to depart straight out until reaching an altitude of 100 ft above ground level nearly 1900 ft from liftoff. The aircraft trajectory during takeoff roll and climb out is plotted in Figure 9.

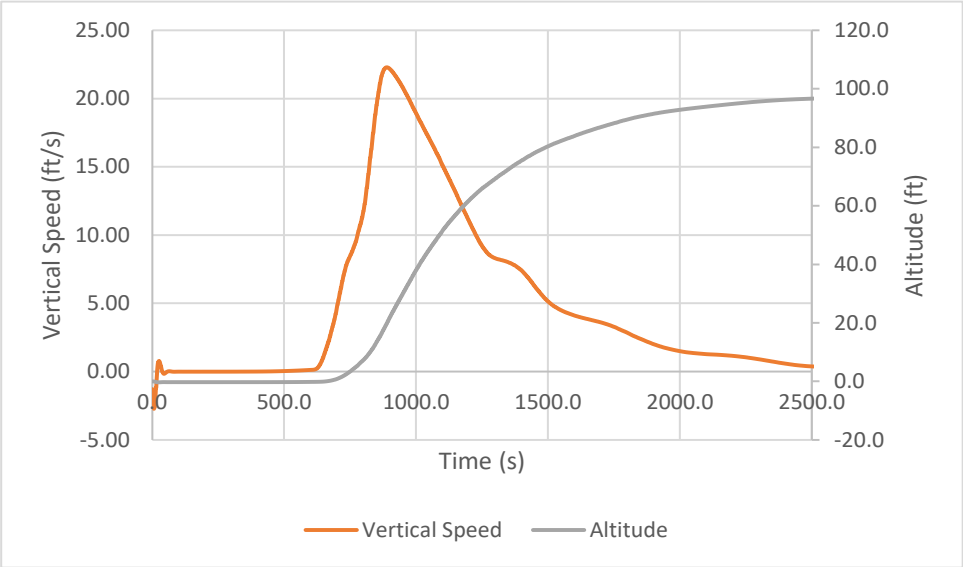

Figure 9: Departure Profile

Longitudinal behavior

Aircraft longitudinal behavior during takeoff can be seen in Figure 10.

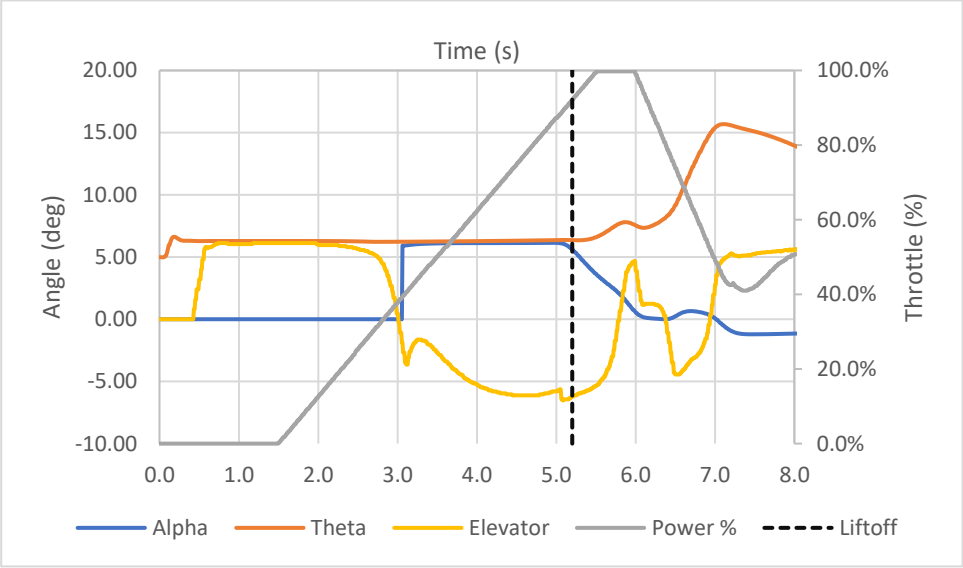

Figure 10: Longitudinal Compensation during Takeoff and Departure

Below 1 ft/s, simulated aircraft sensors do not calculate flight path angles, therefore a jump in α is seen at 3 seconds.

Lateral-Directional behavior

In Figure 11, both rudder and aileron work to try and keep the magnitude of β under 1°. This is significantly better than the initial model, which reached simulated β angles between 5° and 6°. Max rudder and aileron deflections are $\pm 20°$ for the simulation model. This was set to a higher value compared to the anticipated real deflection limits to determine what amount might be more ideal to control the aircraft.

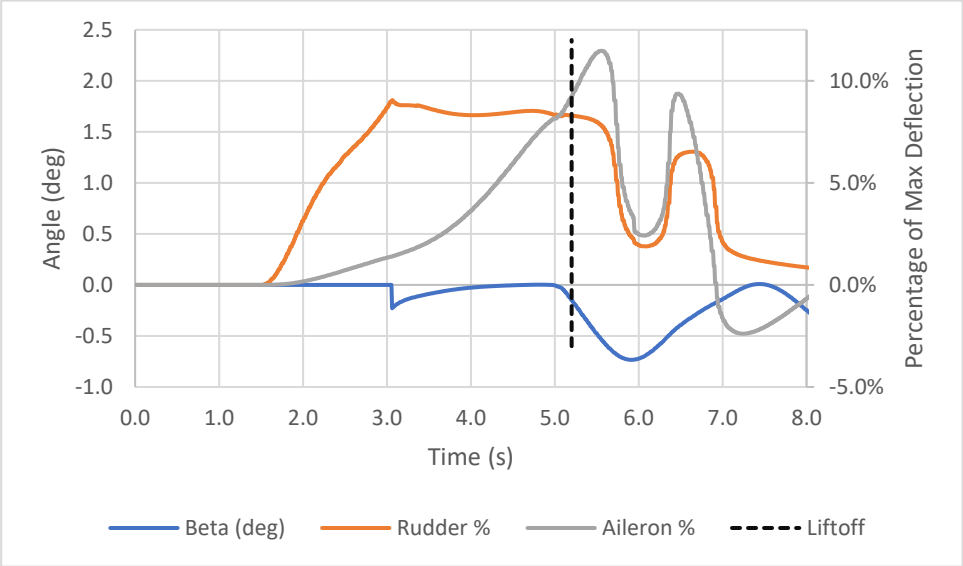

Figure 11: Lateral-Directional Compensation during Takeoff

The aircraft behavior during ground roll is seen Figure 12. Here β is only measured at a velocity above 1 ft/s, hence the spike around 3 seconds. This spike is from propulsion forces as throttle is quickly advanced during takeoff.

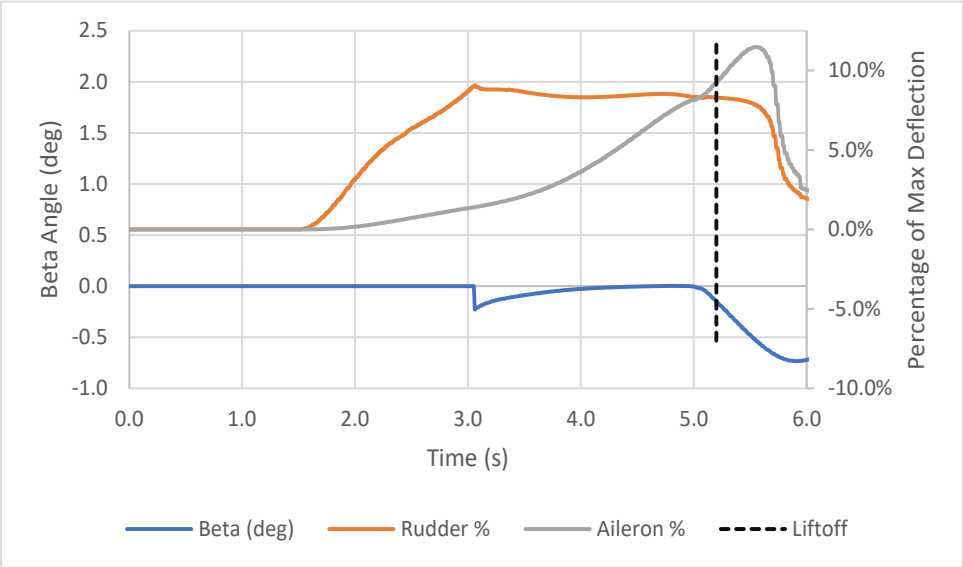

Figure 12: Beta Angle during Ground Roll

After liftoff, β quickly begins to increase as the aircraft rotates to higher pitch angle and asymmetrical blade effects at high angle of attack become a factor.

4.1.2 Final Approach and Landing

Final approach and landing was simulated by commanding the aircraft to begin the approach at 50 ft/s, 50ft above the ground, 850 ft from the desired touchdown point. After passing that waypoint, the aircraft begins to slow to 37 ft/s as it nears the runway. In Figure 13, the aircraft reduces its vertical speed, trying to reach the commanded vertical speed of 0 ft/s just above the runway. This iteration of the Rascal 168 model does not reach a vertical speed lower in magnitude than 1.2 ft/s before touchdown.

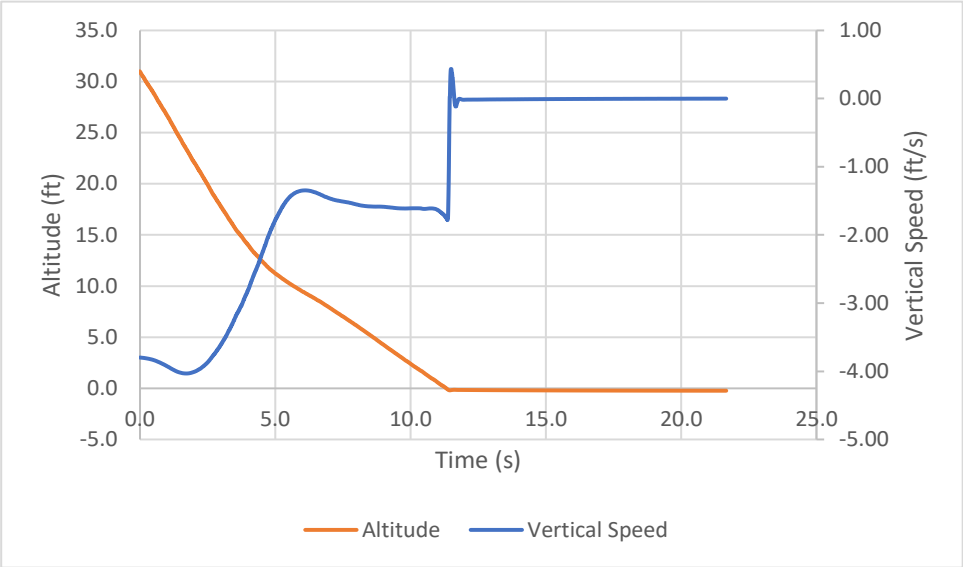

Figure 13: Approach Profile

Longitudinal behavior

Figure 14 shows the resulting angle of attack and pitch angle from elevator deflection and power setting from 20 ft agl to the time of a complete stop on the ground.

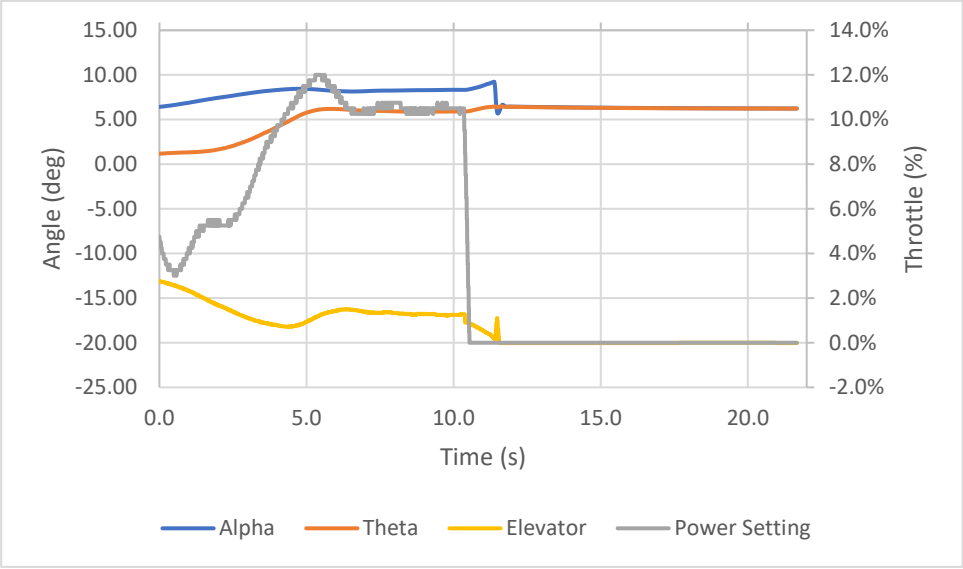

Figure 14: Longitudinal Compensation during Flare and Ground Roll

The aircraft attitude at 2 ft agl and a true airspeed of 36 ft/s during flare is shown in Figure 15.

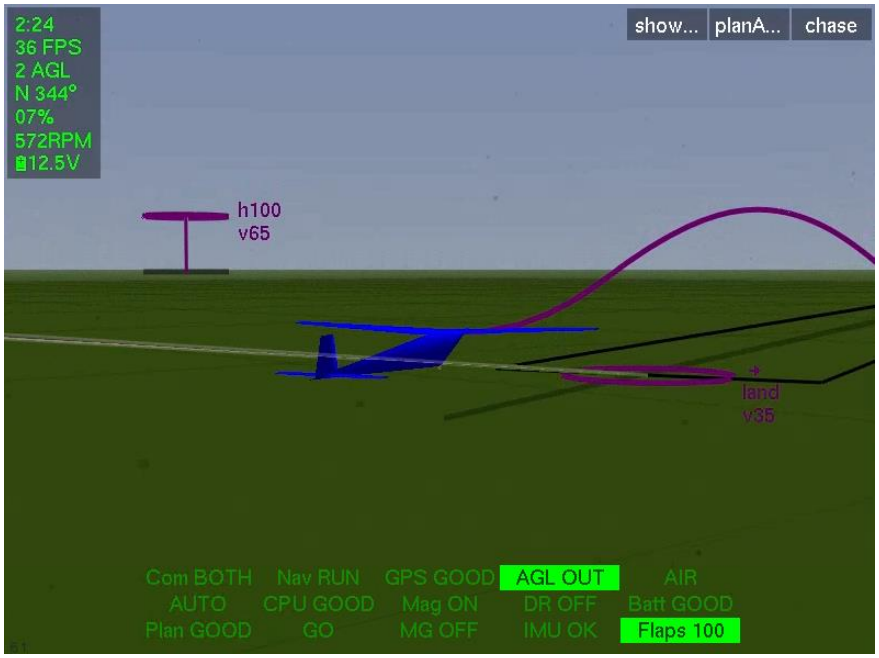

Figure 15: Simulated Flare Transition

In Figure 16, Figure 17, and Figure 18, the Rascal 168 approach profile and that of a fixed-wing aircraft with tricycle landing gear, already implemented in PS/GUST, are compared. Both airplanes are commanded to follow their typical traffic pattern and approach profile around the landing area. Vehicle behavior is recorded from a height of 50 ft on approach until a complete stop is made at the end of the runway. The tricycle gear airplane flies an approach with a steeper glideslope, touches down at a lower vertical speed, and has a significantly longer landing roll than the Rascal 168. As desired, the Rascal 168 reaches a higher angle of attack during flare and touchdown compared to the tricycle gear airplane (Figure 16). This allows the Rascal 168 to reach slower touchdown velocity and better maintain lateral directional control.

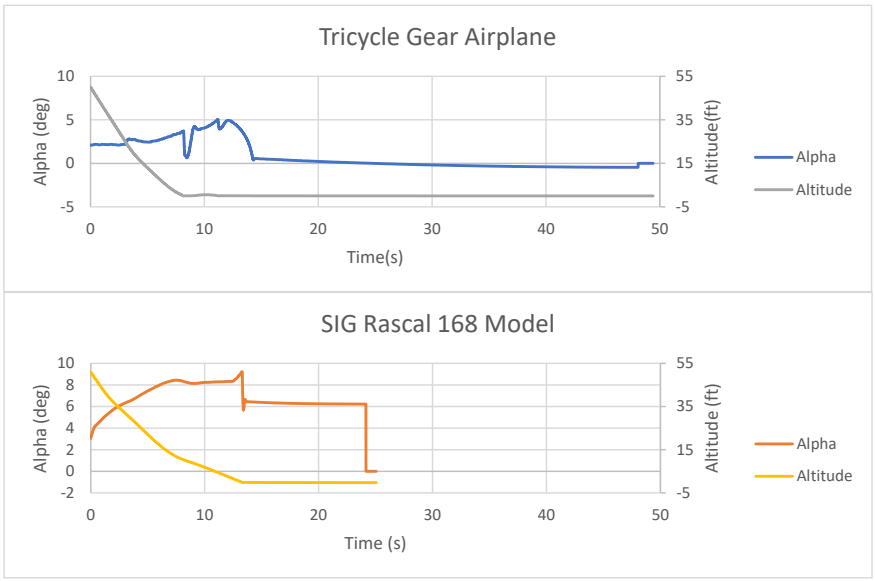

Figure 16: Angle of Attack Comparison on Approach between a Tricycle Gear Airplane and Rascal 168

Figure 17: True Airspeed Comparison on Approach between a Tricycle Gear Airplane and Rascal 168

In Figure 18, the Rascal 168 touchdown vertical speed is observed to be roughly double that of the tricycle gear airplane.

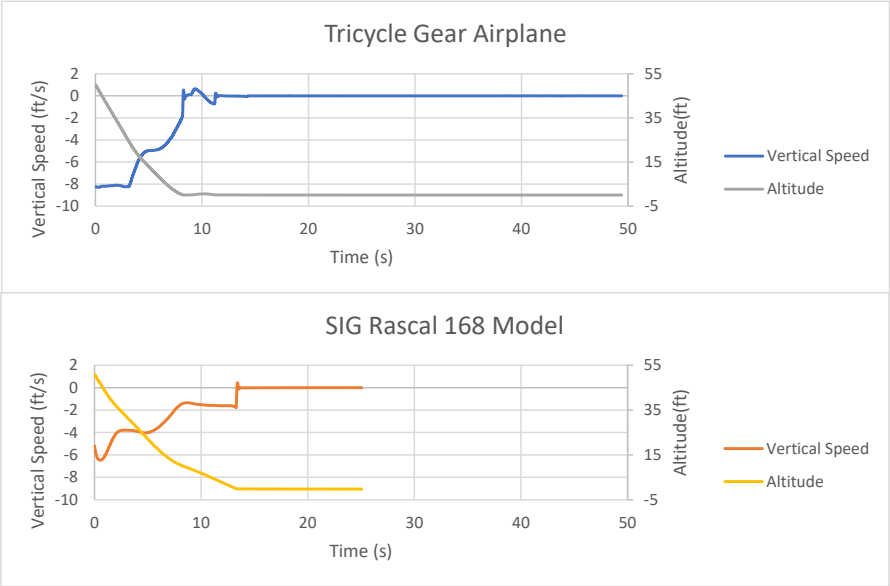

Figure 18: Vertical Speed Comparison on Approach between a Tricycle Gear Airplane and Rascal 168

Since Rascal 168 is approaching the runway with much less momentum at a higher angle of attack, it's harder for the controller to manage vertical speed in the flare. The tricycle gear airplane in PS/GUST touches down with near zero pitch angle at an airspeed well above stall velocity. This allows it to better minimize vertical speed at touchdown.

Lateral-Directional behavior

As explained in Section 3.2.4, a key aspect of tailwheel control on the ground involves minimizing steady state error in β and quick control response when $\dot{\beta}$ is not zero as slight perturbations are encountered. The correlation between power setting, angle of attack, and sideslip angle is depicted in Figure 19.

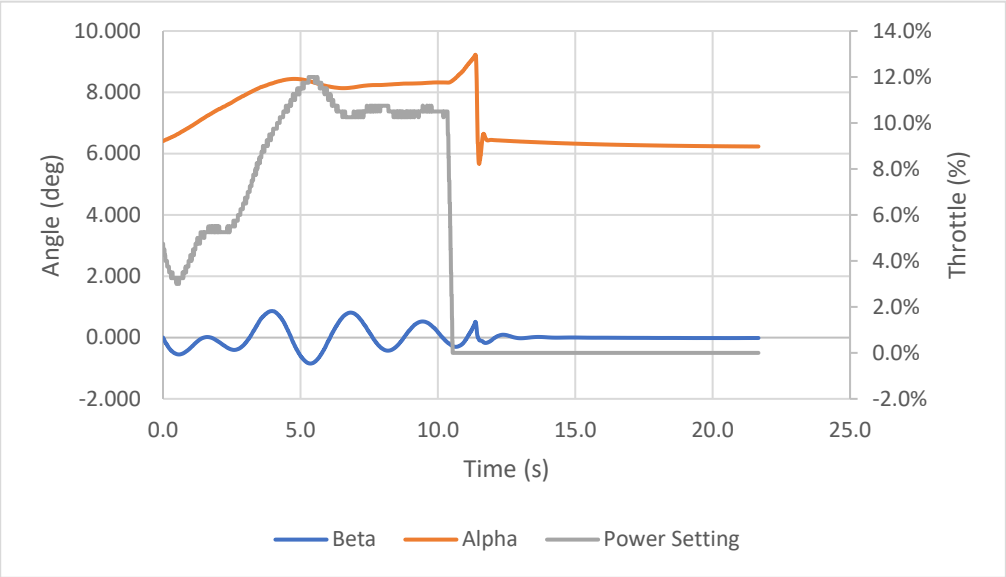

Figure 19: Flight Path Angles and Power Setting during Flare Transition and Ground Roll

Oscillation in sideslip angle closely matches the phase of oscillation of both angle of attack and power setting. This is consistent with the anticipated slipstream effects and asymmetrical propeller loading at a high angle of attack. The simulated lateral-directional control response of the Rascal 168 during approach, flare, and ground roll is shown in Figure 20.

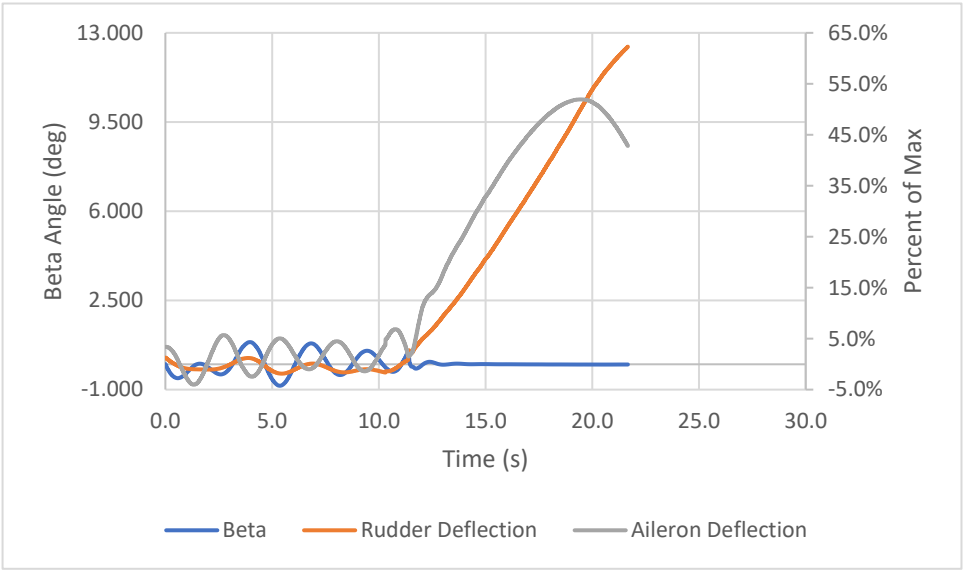

Figure 20: Lateral-Directional Compensation during Approach and Ground Roll

During flare, the controller keeps β under 1 degree in either direction and attempts to maintain runway centerline. During ground roll, both rudder and aileron continue compensating as the airplane decelerates and control effectiveness is lost as seen in Figure 20. In Figure 21, force in the y-direction is minimized before and after touchdown. The jump in force indicates the exact moment of touchdown when the gear absorb any side load at touch down.

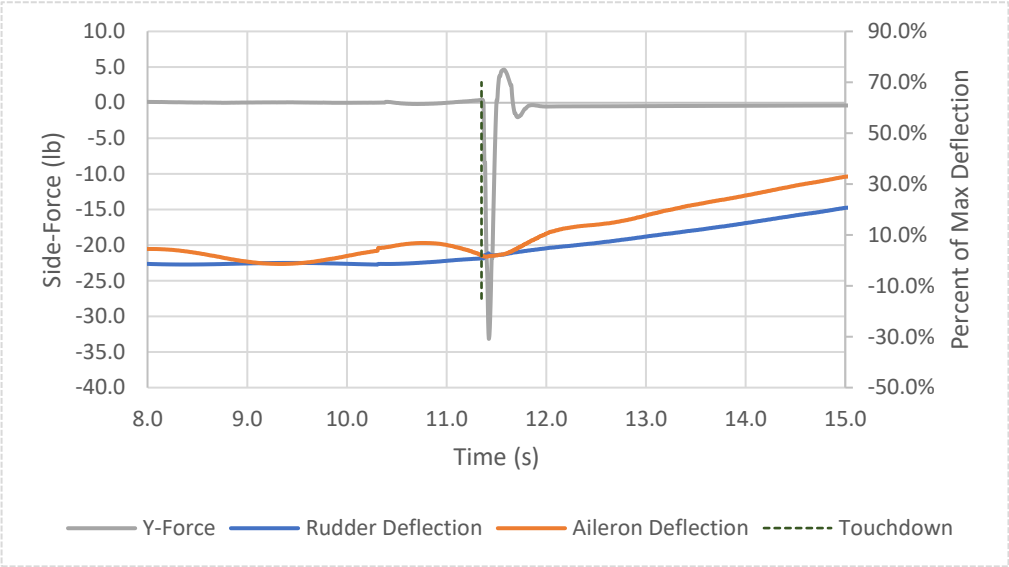

Figure 21: Side Force Compensation during Flare and Touchdown

The importance of even a small sideslip angle can be seen in Figure 21, where the simulated gear load jumps to nearly 47 lbs. The real-world force on the landing gear is heavily dependent on its spring constant. The aircraft orientation at 26 ft/s on the ground is shown in Figure 22.

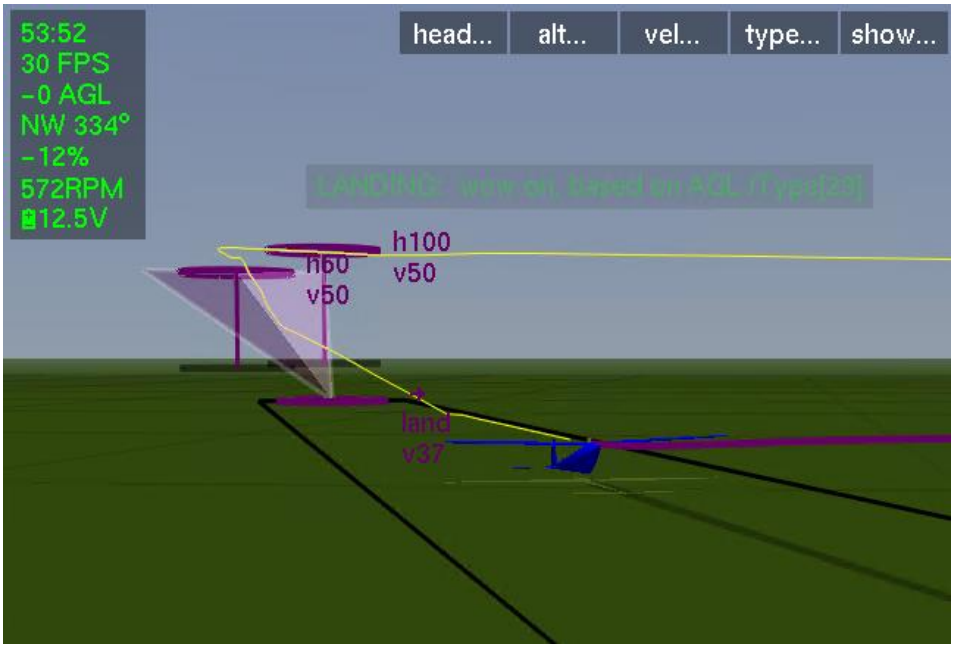

Figure 22: Aircraft Orientation during Simulated Landing Roll

4.2 Manual Flight Test Results

To prepare for the future integration of the flight control solution on the Rascal 168, the assembled aircraft was manually flight tested (Figure 23). The manual flight test was performed at Mid-State Regional Airport (KPSB) on a rough paved surface with a quartering headwind between 10 and 15 mph. During taxi testing, the aircraft was very hard to control at slow speeds on the ground. The high wind conditions made the aircraft weathervaning tendency very obvious while taxing.

Figure 23: SIG Rascal 168 Manual Approach and Flare Transition

The aircraft was flown in a right-hand rectangular pattern at roughly 200 ft around the runway as shown in Figure 24.

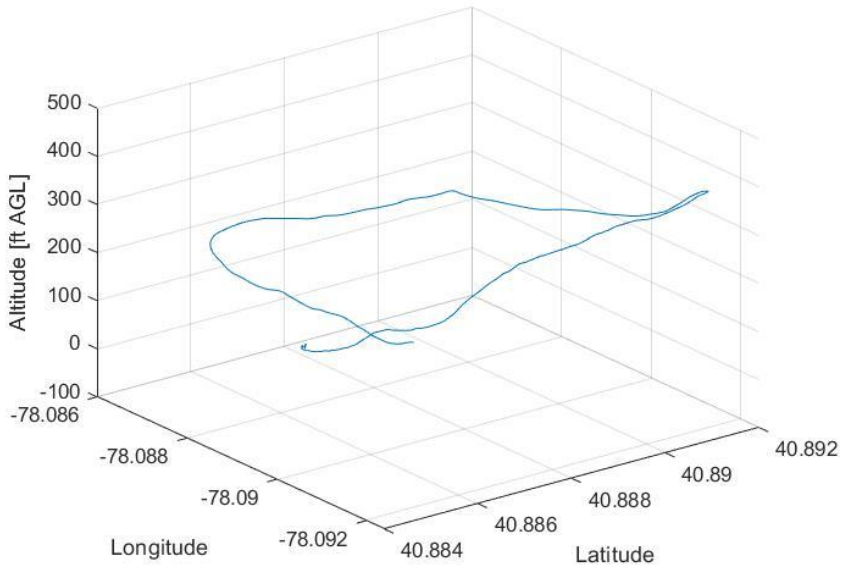

Figure 24: SIG Rascal 168 Manually Flown Flight Path

The recorded ground speed of the aircraft over one circuit is seen in Figure 25.

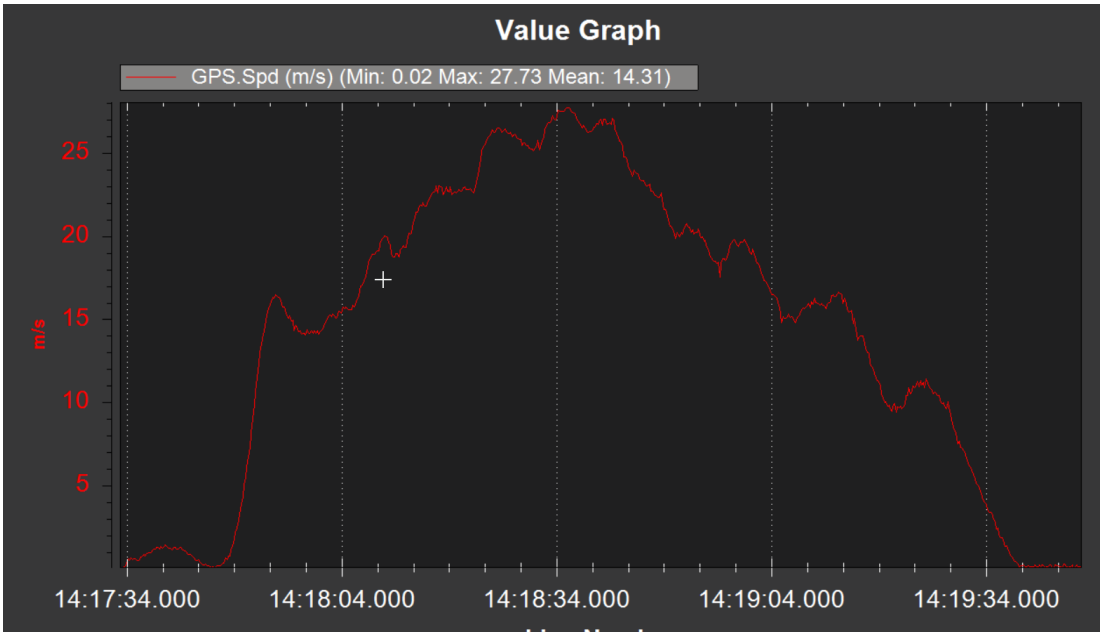

Figure 25: Ground Speed vs Time during Manual Flight Test

Ground speed and estimated wind data was used to approximate the cruise velocity at 50% throttle. When traveling downwind between 150 ft and 250 ft, the aircraft reached a ground speed of 28 m/s. Assuming the winds aloft to be 20 mph or greater from the same direction as ground level, the aircraft cruise speed at half throttle was at most 60 ft/s (40 mph). This behavior was consistent with the propulsion information and drag estimation implemented in the simulation model. Recorded motor setting, altitude, and pitch angle over a single circuit are detailed in Figure 26. The red line indicates the pulse-width modulation (pwm) output associated with the motor. All servo pwm values fall between 1100 and 1900, 1100 being zero percent deflection and 1900 being 100%.

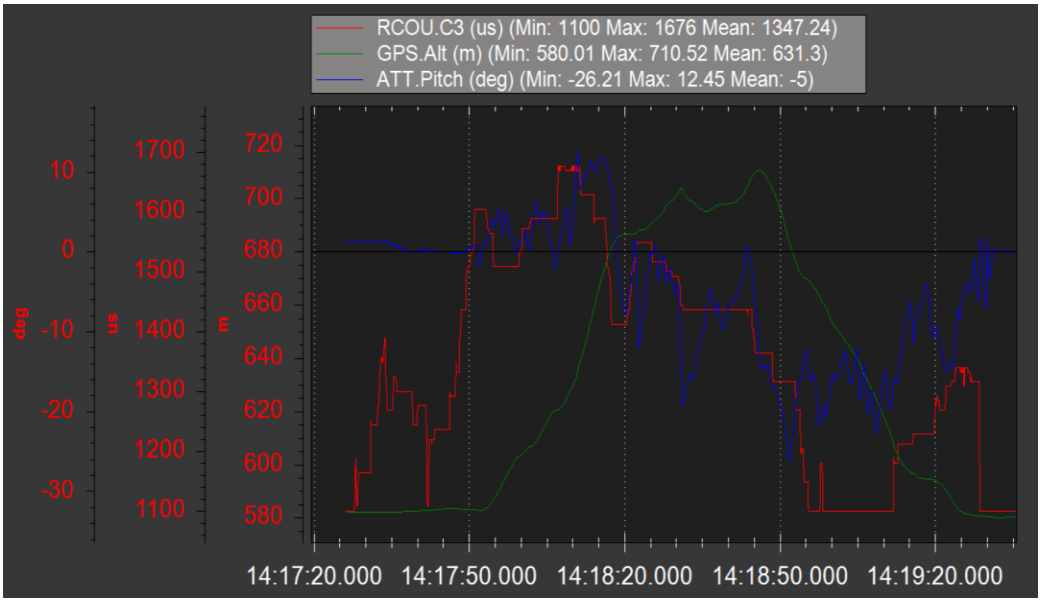

Figure 26: Pitch, Power, and Altitude during Manual Flight Test

The green curve indicates altitude and the blue curve records pitch angle relative to the attitude at system initialization. In Figure 27, the longitudinal control inputs of a human RC pilot are displayed with a significant wind. This information could be used in a qualitative comparison with the simulated controller response in Figure 10 and Figure 14.

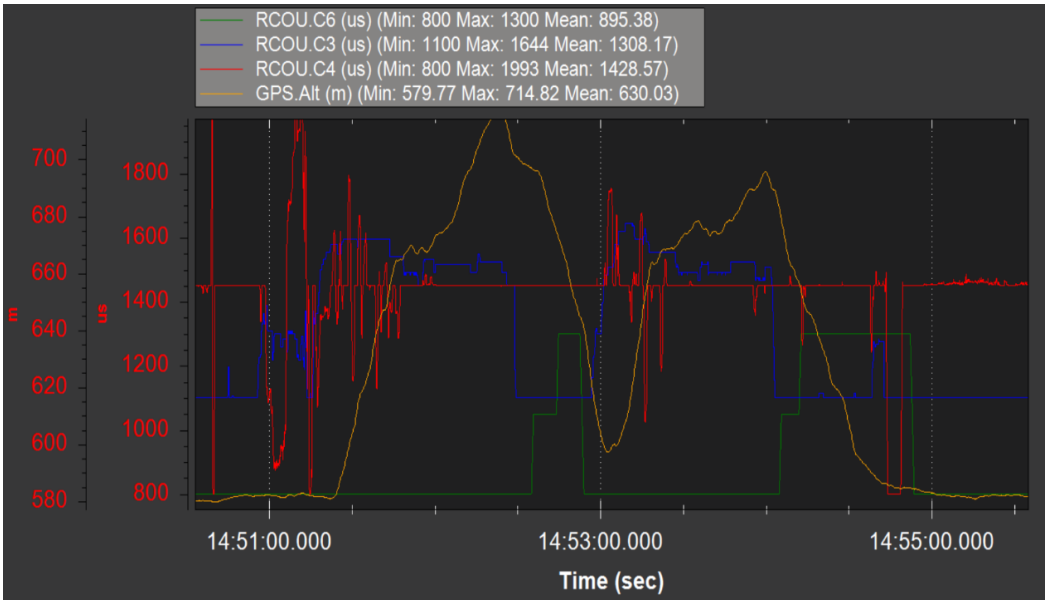

Figure 27: Flap Setting, Throttle Setting, Rudder Deflection, and Altitude during Manual Flight Test

Roll rate was evaluated by fully deflecting the ailerons and noting the amount of time required to bank to roughly 45 degrees. In Figure 28, these intentional jumps in roll angle can be seen at time 14:51:30, 14:51:32, 14:51:39, and 14:51:42. The roll rate from full aileron deflection for each of these manuevers averaged 35 degrees per second.

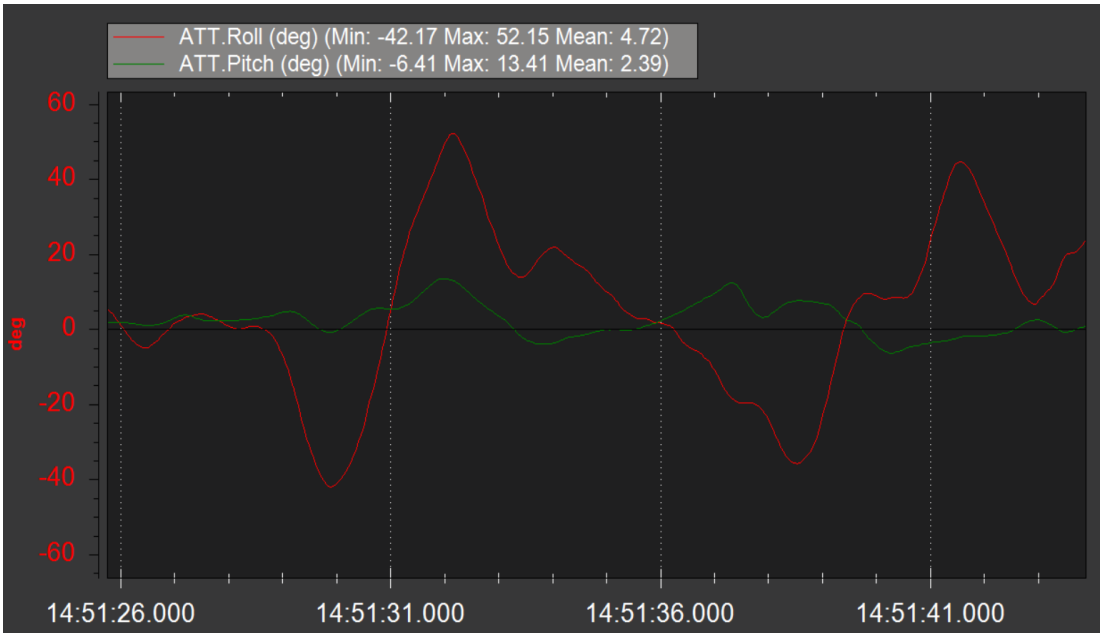

Figure 28: Pitch and Roll vs Time during Manual Flight Test

Since the Rascal 168 roll rate was not investigated in AVL, this information was useful to further improve the accuracy of simulation model in PS/GUST.

Chapter 5:

Conclusion

The flight control solution described in this work has been shown in simulation to adequately compensate for the unique control challenges posed by the SIG Rascal 168 tailwheel aircraft. During takeoff and landing, the controller better minimized steady-state sideslip error and compensated for perturbations when compared to other fixed-wing models in PS/GUST. The aircraft was prepared for autonomous flight test by verifying the validity of the simulation model during a manual flight test.

Future work includes demonstrating the autopilot solution onboard Rascal 168 and gathering autonomous flight test data. Before that can be accomplished, controller response to varying wind conditions should be further investigated within PS/GUST. Aircraft behavior during manual flight test made it clear that the control surface authority required to maintain control of the aircraft changed significantly with a wind shift of just a few knots. Precise air data collection will be required for the controller to precisely fly the commanded approach profiles. Much of the lateral-directional control of the aircraft depends on accurate measurement of sideslip angle. The aircraft implementation in PS/GUST, presented in this thesis, provides a useful starting point for the PURL team to further develop their IARC vehicle solution. This work will also assist with future autonomous implementation of research vehicles with conventional landing gear at PURL.

Appendix A

Nomenclature

AR	=	wing aspect ratio
M	=	pitching moment
N	=	yaw moment
P	=	roll rate
Q	=	pitch rate
R	=	yaw rate
S	=	wing reference area
U	=	absolute velocity component in x-direction
V	=	absolute velocity component in y-direction
W	=	absolute velocity component in z-direction
Y	=	total force in y-direction
b	=	wing span
i	=	wing incidence angle
l	=	roll moment
m	=	mass
r	=	propeller radius
α	=	angle of attack
β	=	angle of sideslip
θ	=	pitch angle
λ	=	wing taper ratio
ϕ	=	bank angle
$C_{M_{\delta_e}}$	=	change in pitching moment coefficient per elevator deflection
C_{M_0}	=	pitching moment coefficient at $\alpha = 0$
C_{M_Q}	=	change in pitching moment coefficient per pitch rate
C_{M_α}	=	change in pitching moment coefficient per alpha
$C_{N_{\delta_r}}$	=	change in yawing moment coefficient due to rudder deflection
C_{N_P}	=	change in yawing moment coefficient per roll rate
C_{N_R}	=	change in yawing moment coefficient per yaw rate
C_{N_β}	=	change in yawing moment coefficient per β
C_{Y_P}	=	change in y-force coefficient per roll rate
C_{Y_R}	=	change in y-force coefficient per yaw rate
C_{Y_β}	=	change in y-force coefficient per β
$C_{l_{\delta_r}}$	=	change in rolling moment coefficient per rudder deflection

C_{l_P}	=	change in rolling moment coefficient per roll rate
C_{l_R}	=	change in rolling moment coefficient per yaw rate
C_{l_β}	=	change in rolling moment coefficient per β
J_X	=	moment of inertia about x-axis
J_{XZ}	=	product of inertia in xz-plane
J_Y	=	moment of inertia about y-axis
J_Z	=	moment of inertia about z-axis
P_{max}	=	maximum input power
Q_{max}	=	maximum motor torque
S_{ht}	=	horizontal tail area
S_{vt}	=	vertical tail area
X_A	=	aerodynamic force in x-direction
X_T	=	thrust force in x-direction
Y_A	=	aerodynamic force in y-direction
Y_T	=	thrust force in y-direction
Z_A	=	aerodynamic force in z-direction
Z_T	=	thrust force in z-direction
b_{ht}	=	horizontal tail span
b_{vt}	=	vertical tail span
$c_{l_{max}}$	=	two-dimensional maximum lift coefficient
$c_{r_{ht}}$	=	horizontal tail root chord
$c_{r_{vt}}$	=	vertical tail root chord
$c_{t_{ht}}$	=	horizontal tail tip chord
$c_{t_{vt}}$	=	vertical tail tip chord
$\bar{c}$	=	mean aerodynamic chord
c_L	=	three-dimensional lift coefficient
c_l	=	two-dimensional lift coefficient
c_r	=	wing root chord
c_t	=	wing tip chord
g_D	=	gravitational acceleration (down)
k_{d_β}	=	rudder deflection per $\dot{\beta}$
k_{d_α}	=	elevator deflection per $\dot{\alpha}$
k_{d_ϕ}	=	aileron deflection per P
$k_{i_{a_x}}$	=	integral gain on acceleration in the x-direction
$k_{i_{a_y}}$	=	integral gain on acceleration in the y-direction
$k_{i_{a_z}}$	=	integral gain on acceleration in the z-direction
k_{i_α}	=	integral gain on elevator
k_{i_β}	=	integral gain on rudder
k_{i_ϕ}	=	integral gain on aileron

$k_{p_{a_x}}$	=	thrust per acceleration in the x-direction
$k_{p_{a_y}}$	=	$\frac{\beta}{\text{lateral acceleration}} * (\text{velocity})^2$
$k_{p_{a_{y_G}}}$	=	$k_{p_{a_y}}$ at 130% of flare rotation velocity
$k_{p_{a_z}}$	=	$\frac{\alpha}{\text{vertical acceleration}} * (\text{velocity})^2$
k_{p_β}	=	rudder per β
k_{p_α}	=	elevator per α
k_{p_ϕ}	=	aileron per ϕ
k_{ar}	=	aileron and rudder interconnect
k_d	=	derivative gain
k_i	=	integral gain
k_p	=	proportional gain
k_q	=	elevator per pitch rate
$\bar{y}$	=	mean aerodynamic chord location
δ_e	=	elevator deflection
δ_r	=	rudder deflection
θ_1	=	propeller twist
Ω	=	propellor angular velocity

REFERENCES

[1] Drela, M., and Youngren, H., “AVL Overview”, Massachusetts Institute of Technology [online], 2008, http://web.mit.edu/drela/Public/web/avl/. [retrieved 6 April 2021]

[2] O’Toole, Sean, "Development of a Remotely-Piloted Vehicle Platform to Support Implementation, Verification, and Validation of Pilot Control Systems" (2017). Dissertations and Theses. 372. https://commons.erau.edu/edt/372.

[3] Jodeh, Nidal, Paul Blue, and Athon Waldron. “Development of Small Unmanned Aerial Vehicle Research Platform: Modeling and Simulating with Flight Test Validation.” AIAA Modeling and Simulation Technologies Conference and Exhibit. Keystone, Colorado: American Institute of Aeronautics and Astronautics, 2006. https://doi.org/10.2514/6.2006-6261.

[4] Drela, M., and Youngren, H., “XFOIL”, Massachusetts Institute of Technology [online], 2013, https://web.mit.edu/drela/Public/web/xfoil/. [retrieved 6 April 2021]

[5] Stevens, Brian L., Frank L. Lewis, and Eric N. Johnson. *Aircraft Control and Simulation: Dynamics, Controls Design, and Autonomous Systems: Dynamics, Controls Design, and Autonomous Systems.* Hoboken, NJ, USA: John Wiley & Sons, Inc, Hoboken, NJ, USA: 2015, pp. 63–141. doi:10.1002/9781119174882.ch2.

[6] Johnson, Eric N. “Georgia Tech UAV Simulation Tool (GUST) Overview.” 2016.

[7] Johnson, Eric N., and Daniel P. Schrage. “System Integration and Operation of a Research Unmanned Aerial Vehicle.” *Journal of Aerospace Computing, Information, and Communication* Vol. 1, No 1, (January 2004): 5–18. https://doi.org/10.2514/1.4424.

[8] Johnson, Eric N., and Anthony J. Calise. “Limited Authority Adaptive Flight Control for Reusable Launch Vehicles.” *Journal of Guidance, Control, and Dynamics* Vol. 26, No. 6 (November 2003): 906–13. https://doi.org/10.2514/2.6934.

[9] Johnson, Eric N., and Anthony J. Calise. "Pseudo-control hedging: A new method for adaptive control." *Advances in navigation guidance and control technology workshop*, pp. 1-2. Alabama, USA Alabama, USA, 2000.

ACADEMIC VITA

Gracelyne H. Allred

EDUCATION

Bachelor of Science in Aerospace Engineering

Schreyer Honors College Graduation: May 2021

The Pennsylvania State University, University Park, PA

Software: XFLR5, AVL, SolidWorks, C++, MATLAB, ArcGIS

TECHNICAL EXPERIENCE

Aerodynamics Engineering Intern May - August 2020

The Boeing Company, Seattle, WA

- Formulated high lift and configuration changes for a market competitive aircraft derivative
- Refined desired aircraft design points using a rapid configuration analysis and optimization tool
- Facilitated team meetings and discussion as changes were integrated into a cohesive solution

Flight Deck Crew Operations and Integration Intern June - August 2019

The Boeing Company, Seattle, WA

- Analyzed flight profiles and assessed pilot feedback to reduce pilot workload
- Evaluated system failure modes and effects to optimize aircraft display interface
- Coached peers through flight deck operational processes and design philosophy

Lab/Teaching Assistant - Intro to Engineering Design August 2018 – May 2020

Penn State Student Support Services, University Park, PA

- Guided 150+ students through the design process and prototype development

Aircraft Mechanic's Assistant June 2013 - August 2016

Private employer, Selinsgrove, PA

- Assisted an A&P Mechanic with the maintenance of various single engine aircraft

PROJECTS

AIAA Design Build Fly Competition August 2018 - May 2020

Penn State DBF Team Lead

- Led team through the design and build of a competitive RC airplane within mission constraints
- Compiled trade studies, analysis results, and performance predictions in a 60-page design report

PSU Sailplane January 2018 - Present

Teaching Intern, PSU Zephyrus

- Guided students through the fabrication and design of a composite human-powered aircraft
- Expanded construction experience in carbon fiber layups and wing section construction

INTERNATIONAL EXPERIENCE

Ecole Centrale de Nantes May 2019

School of Engineering Design, Nantes, France

- Explored how cultural context and lifecycle awareness impacts human centered design

ACTIVITIES

Private Pilot – Airplane Single Engine Land, Glider May 2016 - Present

- Building hours towards SEIR and Commercial certificate

Mentor, Women in Engineering Program Orientation Leadership Team August 2019 - Present

- Modeled positive academic outcomes and career development for first-year women
- Provided yearlong support to 14 first-year women to increase engineering retention

Penn State Soaring Club August 2017 - Present

- Expanding experience maintaining, flying, and restoring sailplanes